

## A TG ANALYSIS OF THE EFFECT OF CALCINATION CONDITIONS ON THE PROPERTIES OF REACTIVE MAGNESIA

B. Liu, P. S. Thomas, A. S. Ray\* and J. P. Guerbois

Department Chemistry, Materials and Forensic Sciences, University of Technology Sydney, PO Box 123, Broadway NSW 2007, Australia

The reactivity of MgO obtained from calcination of magnesium carbonate at different temperatures has been investigated by means of hydration in a constant relative humidity environment at 40°C for periods up to 24 days. Natural magnesite and AR grade basic MgCO<sub>3</sub> calcined in the range of 500–1000°C was characterised in terms of surface area, crystallite size, morphology, and hydration rate.

It was found that the hydration rate is dependent on the surface area and crystallite size where temperature was the main variable affecting them. The most reactive MgO was produced at the lowest calcination temperature with the highest surface area and the smallest crystallite size. The basic MgO specimens showed higher degree of hydration compared to the natural MgO specimens due to the smaller surface area and larger crystallite size. The low MgO content of the starting natural magnesite is also attributable to the lower reactivity. This preliminary study serves as a mean to investigate potential utilisation of reactive MgO as a supplementary cementitious material in eco-friendly cements.

**Keywords:** brucite, calcination, hydration, magnesia, magnesite

### Introduction

Of all the known magnesium minerals, magnesia (MgO) is considered the most commercially important magnesium compound [1–3]. The main sources of MgO are from natural magnesium carbonate ore (magnesite) and through recovery from seawater and brines. Magnesia has a wide variety of applications ranging from cattle feed, antacid treatment for humans and animals to environmental control; but its principal use is in refractory bricks and refractory coatings used to produce steel. Magnesia is mostly produced by calcination of magnesite where physical properties of the final magnesia are dependent on the calcination conditions. Increase in calcination temperature is accompanied by increase in the MgO crystallite sizes but a decrease in porosity, surface area, and reactivity [3]. The reactivity of magnesia can, therefore, be controlled to suit the intended applications. For its use in refractories for steel production, a highly crystalline form of magnesia, commonly called periclase or dead-burned MgO, produce in temperatures in excess of 1800°C is used for its exceptional resistance to hydration, hence resistance to degradation. In contrast, light-burned reactive magnesia, typically produced at 600–900°C, is characterised by a small crystallite size, relatively high surface area and a moderate to high chemical reactivity. Reactive magnesia readily hydrates on contact with water even in cementitious environments, hence, its

potential use as a supplementary cementitious material (SCM) where energy required for its production compared to cement (typically produced at 1400°C) is considerably lower.

The reactivity of light-burned magnesia is influenced to a great extent by several factors such as its origin, presence of impurities, and most importantly the temperature it has been subjected to [4]. Thus, this paper investigates the effect of calcination conditions on the reactivity of the magnesia to hydration rate. The reactivity of differently calcined natural magnesite and AR grade basic MgCO<sub>3</sub> in the temperature range of 500–1000°C was characterised by gravimetric methods after hydrating under atmosphere of controlled relative humidity. The degree of hydration was subsequently determined by the TG analysis of the dehydroxylation of the brucite (Mg(OH)<sub>2</sub>) formed.

### Experimental

#### Materials

#### Raw materials

Raw materials used in this study are listed as follows:

- Natural magnesite supplied by Unimin Australia Limited, Sydney, Australia with a bulk density of 1.6 g cm<sup>-3</sup> and a particle size range of less

\* Author for correspondence: A.Ray@uts.edu.au

than 75  $\mu\text{m}$  with a maximum of 2% greater than 75  $\mu\text{m}$ . From X-ray fluorescence analysis the natural magnesite contained 80.20% MgO, 2.91%  $\text{Al}_2\text{O}_3$ , 11.18%  $\text{SiO}_2$ , 2.11% CaO and 1.09%  $\text{Fe}_2\text{O}_3$ .

- AR grade light basic magnesium carbonate ( $4\text{MgCO}_3 \cdot \text{Mg}(\text{OH})_2 \cdot 4\text{H}_2\text{O}$ ),  $\geq 98.5\%$  with CaO (0.4% max) and  $\text{SO}_4$  (0.2% max) as the major impurities, was supplied by Sigma-Aldrich (Australia). The bulk density of the basic carbonate was  $0.083 \text{ g cm}^{-3}$  and had a particle size range of less than 50  $\mu\text{m}$  with a maximum of 2% greater than 50  $\mu\text{m}$ .

### Sample preparation

In order to obtain 15 g of MgO after calcination, mass loss data at  $1000^\circ\text{C}$  were used to calculate the mass of each starting carbonate; 28.39 g of the natural magnesite and 35.24 g of the basic  $\text{MgCO}_3$ . Calcination of each carbonate was carried out simultaneously i.e. at the same time under the same conditions. The specimens were then held at the calcination temperature in the range  $500\text{--}1000^\circ\text{C}$  at  $100^\circ\text{C}$  intervals for 6 h before allowing the specimens to naturally cool. During the cooling process the calcined samples were removed from the furnace at approximately  $250^\circ\text{C}$  and left to cool to room temperature in a desiccator. Each specimen was designated according to its origin (N=natural and B=basic) followed by the calcination temperature.

The RH chamber used for the hydration of differently calcined MgO samples consisted of a glass container with freshly prepared aqueous salt solution of  $\text{KNO}_3$  equilibrated at  $40^\circ\text{C}$  in a fan oven. Under these conditions, a constant RH of  $89.0 \pm 1.2\%$  was expected [5]. The measured RH% was observed to be significantly lower than this value. The RH was measured at 60% after 24 h of exposure rising to a value of 80% after 6 days and remained at 80% for the remainder of the hydration period. The low values observed are likely to be associated with the consumption of atmospheric moisture by the calcined magnesia specimens during hydration process. As the rate of hydration is a function of the humidity, absolute hydration rate measurement was not feasible due to the variance in RH%. However, as all specimens were treated in an identical manner, a relative measure of the reactivity of the calcined magnesia to hydration was possible. Specimens of 0.50 g of calcined natural magnesite and 0.10 g of calcined basic  $\text{MgCO}_3$  samples were weighed into polypropylene sample vials ( $\text{Ø}20\text{mm} \times \text{H}25\text{mm}$ ) and tapped down to an even layer to produce a consistent sample height of approximately 3 mm. The difference in sample mass used was due to the bulk density. Samples were then placed in

the RH chamber to hydrate for 1, 2, 4, 8, 16 and 24 days. Samples were immediately dried in an oven at  $110^\circ\text{C}$ , after removal, for minimum of 2 h and then stored in a desiccator overnight before verifying the brucite peak using thermogravimetric analysis.

### Methods

BET surface area by gas adsorption flow-technique of calcined MgO samples was determined using a Philsorb Mk 1 Surface Area Chemisorption Analyser running on 30%  $\text{N}_2$  in helium. The instrument was calibrated by passing 0.5 and 5.0 mL quantities of nitrogen gas to the analytical side of the thermal conductivity detector. The system measures the amount of nitrogen gas adsorbed on the surface of the powder samples by allowing the surface to become saturated with the gas by cooling in liquid nitrogen and then measuring the quantity of gas released when the sample is heated back to room temperature.

SEM was conducted using a LEO Supra 55VP Scanning Electron Microscope (SEM) at an accelerating voltage of 2.0 kV under HiVac mode. Images were captured using an in-lens detector.

XRD analyses were performed using a Siemens D5000 diffractometer operating at 40 kV and 30 mA with  $\text{CuK}_\alpha$  radiation from  $10$  to  $84^\circ 2\theta$  at intervals  $0.02^\circ$ . Step times of 1 s per intervals were used. Powder diffraction data sets were compared to those from the Joint Committee on Powder Diffraction Standards (ICDD-JCPDS) CD-ROM database providing qualitative phase identification. Crystallite sizes were determined by Scherrer method using TOPAS 2.0 with correction for line broadening using a fundamental parameters approach for X-ray line profile fitting [6]. Measurements were confined to the strongest (200) periclase line in the X-ray pattern.

Thermal analyses were performed on  $20 \pm 1.0$  mg natural MgO samples and  $5 \pm 0.5$  mg basic MgO using a TA-instruments' SDT 2960 simultaneous differential thermal analysis and thermogravimetric analysis (DTA-TG) at a heating rate of  $20^\circ\text{C min}^{-1}$  under flowing air ( $20 \text{ mL min}^{-1}$ ) from ambient to  $1000^\circ\text{C}$ . Calcination checks were carried out with the same parameters with the exception of the heating rate at  $10^\circ\text{C min}^{-1}$ .

## Results and discussion

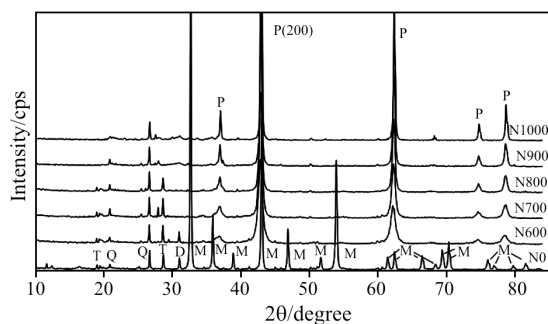
The degree of calcination (Table 1) of each calcined samples was determined by mass loss during decarbonation. The calcination of natural magnesite at  $500^\circ\text{C}$  (N500) was incomplete and therefore was excluded from subsequent hydration experiments. The calcined natural magnesites showed an overall

**Table 1** (i) Degree of calcination based on the mass loss of the decarbonation peak compared to their respective uncalcined raw material. (ii) BET surface area of calcined magnesias and raw materials. (iii) Crystallite size determined from periclase (200) X-ray diffraction line

Calcination temperature/°C	Degree of calcination/%		Surface area/m <sup>2</sup> g <sup>-1</sup>		Crystallite size/nm	
	natural	basic	natural	basic	natural	basic
0	–	–	2.25	34.53	–	–
500	32.06	95.25	–	158.82	–	8.6
600	94.66	98.38	104.23	117.74	16.1	12.5
700	98.24	99.27	71.15	80.46	26.2	19.1
800	98.80	99.84	43.68	49.37	39.6	30.6
900	99.71	99.87	32.49	50.99	57.4	32.4
1000	99.98	99.40	13.25	40.88	98.1	40.4

lower degree of calcination compared to the basic samples. Girgis and Girgis [7] suggested that impurities in the natural magnesite, in particular iron oxide, inhibited the decarbonation during calcination thereby requiring the decomposition to take place at a higher temperature than the pure AR grade basic MgCO<sub>3</sub> for the given conditions.

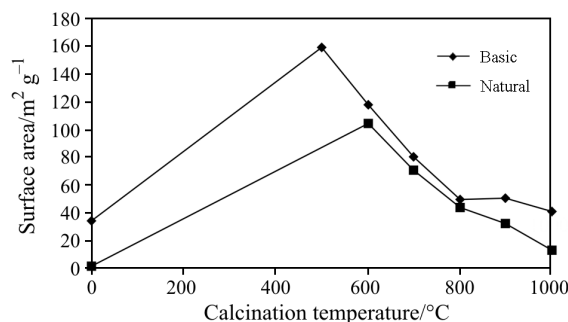
X-ray analysis (Fig. 1) indicated that the natural magnesite is mainly composed of magnesite with small amounts of quartz, dolomite and talc. The main dolomite peak at 2.9 Å was absent in the N700 specimen while the talc peaks disappeared at 900°C. A new peak was observed in the N700 specimen at around 2θ=28° (3.2 Å). This is most likely to be an enstatite (magnesium silicate) peak derived either from the solid-state reaction of magnesium oxide with silica present as an impurity or from thermally treated talc. Periclase peaks are observed to become narrower and they increase in peak heights with increasing calcination temperatures in both series. The peak width is associated with crystallite size where line broadening is caused by very small crystallites. By utilising the Scherrer method, approximate crystallite sizes were determined and are listed in Table 1. Larger crystallite sizes were observed for the natural MgO with more than double the size at 1000°C. This is also reflected in

**Fig. 1** X-ray diffraction patterns of natural magnesite and calcined natural magnesite at 600, 700, 800, 900 and 1000°C. M=magnesite, P=periclase (MgO), T=talc (Mg<sub>3</sub>Si<sub>4</sub>O<sub>10</sub>(OH)<sub>2</sub>), Q=quartz, D=dolomite (CaMg(CO<sub>3</sub>)<sub>2</sub>)

the BET surface area where the increase in crystallite size with increase in calcination temperature resulted in smaller surface area for both specimens.

The BET surface area plots are shown in Fig. 2. Both curves show a substantial increase in surface area most likely due to thermal decomposition leading to smaller crystallites. Calcination processes also aid in the development of porosity with the pseudomorphic transformation from MgCO<sub>3</sub> to MgO [8], hence, higher surface area. The gradual decrease in surface area with increasing calcination temperature was due to the effects of sintering. It is noteworthy that, although a large difference in surface area is observed between the starting materials, the surface areas of the resulting magnesias were quite similar particularly at 600, 700 and 800°C. A large difference in surface area is observed at 900 and 1000°C with both magnesias approaching surface area that of the corresponding starting material. This limit in surface area suggests that sintering at these temperatures may not involve fusion of particles but rather sintering of micropores on individual particles. SEM analysis provided some supporting evidence to this conjecture.

The morphological changes of the MgO crystals are illustrated by the electron micrographs. Figure 3b shows the presence of fine protrusions on the surfaces of MgO particles, thus creating a more porous structure

**Fig. 2** BET surface area of calcined and uncalcined natural magnesite and basic MgCO<sub>3</sub>

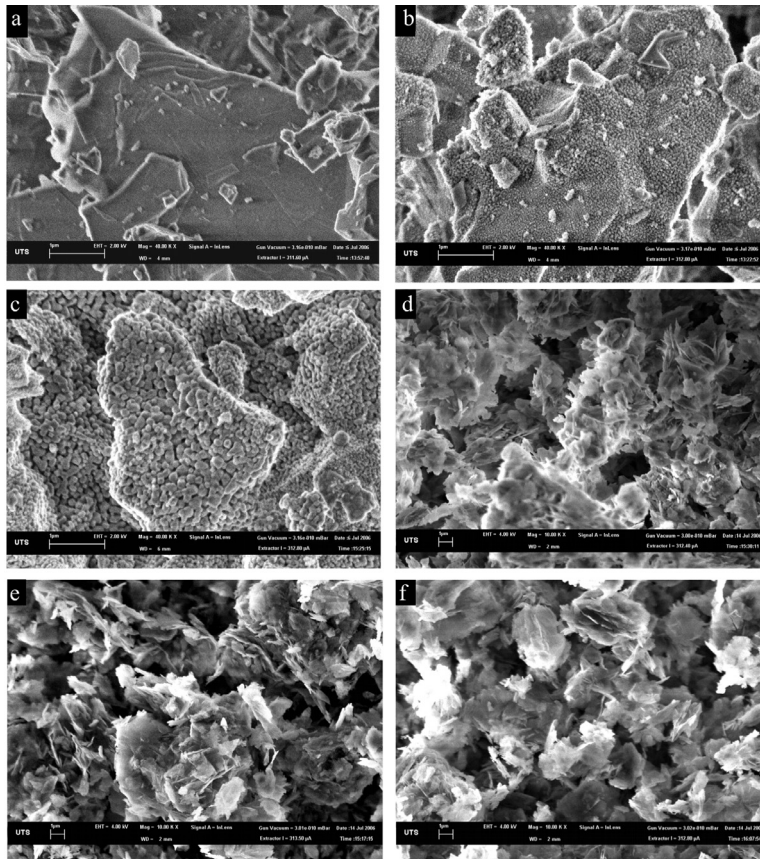


**Fig. 3** SEM micrograph of a – raw natural magnesite, 40000 $\times$ ; b – N600, 40000 $\times$ ; c – N1000, 40000 $\times$ ; d – raw basic  $\text{MgCO}_3$ , 10000 $\times$ ; e – B600, 10000 $\times$ ; f – B1000, 10000 $\times$

with higher surface area. By contrast, the uncalcined magnesite particles had smooth surfaces shown in Fig. 3a. With increasing calcination temperature, the fine protrusions started to grow and fuse together as shown on the micrograph of N1000 (Fig. 3c), indicating the origins of the decrease in the BET surface area. The effect of sintering was not observed in the micrographs of the calcined basic  $\text{MgCO}_3$  samples. The uncalcined basic  $\text{MgCO}_3$  had randomly ordered scaly particles as shown in Fig. 3d. No obvious changes were observed for the entire series of calcined samples (Figs 3e and f), which corresponded to the relatively smaller changes in the crystallite size compared to the natural  $\text{MgO}$ . This may be due to the fact that basic  $\text{MgCO}_3$  had a very low bulk density, and hence had insufficient mass for the sintering process to take place efficiently. This may also be due to the particle shape, size and surface morphology obscuring any observable effects of sintering. The difference in the surface morphology may be due to the restricted surface area in the natural magnesite for the removal of  $\text{CO}_2$  gas resulting in nano-scaled surface rupturing.

Figures 4 and 5 show the degree of hydration as a function of exposure time. For both N and B series, the degree of hydration is a strong function of the calcination temperature with higher temperature resulting in

lower degree of hydration. This is consistent with the BET surface area and the XRD data where reduced surface area and increased crystallinity and crystallite size are inhibiting hydration resulting in lower degree of reactivity. The degree of maximum hydration for both series tends to a limiting value, 70% for the N series and 85–90% for the B series. This difference may be attributed to the impurities in the natural magnesite where, the  $\text{MgO}$  content or the purity of the starting natural magnesite was considerably lower (80.20%). The N600 specimen was not completely calcined (Table 1), hence, it resulted in a slightly lower maximum

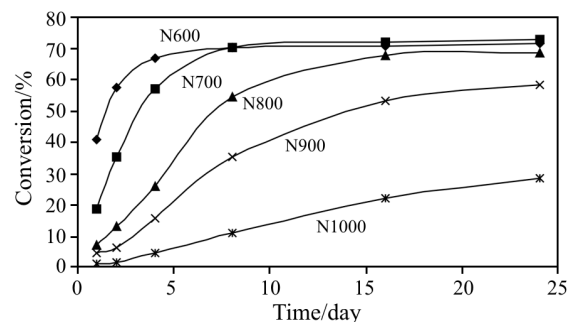


**Fig. 4** Degree of hydration, in a constant RH atmosphere, of calcined natural  $\text{MgO}$  to  $\text{Mg}(\text{OH})_2$

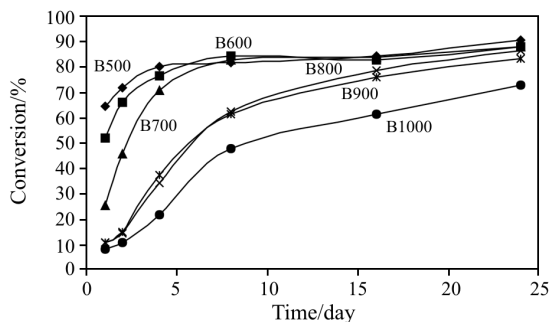


Fig. 5 Degree of hydration, in a constant RH atmosphere, of basic natural MgO to Mg(OH)<sub>2</sub>

conversion than the N700 specimen. Regardless of differences in the initial reaction rates, longer reaction times produced in a constant hydration level of approximately 70% for the natural MgO and approximately 85–90% for the basic MgO.

Examining the first segment of the hydration curves prior to the 4<sup>th</sup> day, two groups of curves are formed segregating between 700 and 800°C, where above 800°C, the initial hydration rate was significantly lower. This occurrence was observed by several authors as discussed by Razouk and Mikhail [4]. However, opinions on the temperature range where such change in the hydration tendency takes place is divided. These temperatures ranged from as low as 800°C, which coincides with the current study, up to 1600°C.

## Conclusions

Calcination temperature has been shown to be a major factor influencing surface area and crystallite size, and thus the reactivity of the calcined magnesite. The surface area was shown to increase significantly due to thermal decomposition leading to the formation of small crystallites as evident from the X-ray line-broadening results. Increasing the sintering temperature resulted in a gradual decrease in surface area as

observed by the morphological changes of the natural magnesite using SEM analysis. The reactivity of the different magnesite was also demonstrated by their rates of hydration in a constant relative humidity environment. The lowest calcination temperatures produced the most reactive magnesite. Basic MgO showed higher reactivity across all temperatures compared to the natural specimens with most reaching above 80% conversion. Neither series achieved complete hydration after 24 days. However, the maximum constant conversion rate for the basic specimens was approximately 90% while the natural specimens only reached approximately 70%, this was primarily due to differences in their reactivity and the fact that MgO content was lower for the natural specimens.

## References

- 1 A. N. Copp, *Am. Ceram. Soc. Bull.*, 77 (1998) 107.
- 2 M. Frith, T. Buffrey and I. Strawbridge, *Br. Ceram. Trans.*, 97 (1998) 29.
- 3 D. A. Kramer, *Am. Ceram. Soc. Bull.*, 80 (2001) 81.
- 4 R. I. Razouk and R. S. Mikhail, *J. Phys. Chem.*, 59 (1955) 636.
- 5 Standard Practice for Maintaining Constant Relative Humidity by Means of Aqueous Solutions, ASTM International, 1996, ASTM E104-85.
- 6 R. W. Cheary and A. Coelho, *J. Appl. Crystallogr.*, 25 (1992) 109.
- 7 B. S. Girgis and L. G. Girgis, *J. Appl. Chem.*, 19 (1969) 292.
- 8 V. S. S. Birchal, S. D. F. Rocha and V. S. T. Ciminelli, *Miner. Eng.*, 13 (2000) 1629.
- 9 R. I. Razouk and R. S. Mikhail, *J. Phys. Chem.*, 62 (1958) 920.
- 10 G. L. Smithson and N. N. Bakhshi, *Can. J. Chem. Eng.*, 47 (1969) 508.
- 11 W. Feitknecht and H. Braun, *Helv. Chim. Acta*, 50 (1967) 2040.

DOI: 10.1007/s10973-006-8106-0